Supporting Information

Layered vanadium oxide with tunable layer spacing via dual organic molecule co-insertion for advanced aqueous zinc-ion batteries

Hong Ding [a,#], Tiantian Li [a,#], Chengyu Liu [a], Jiali Wang [a], Tengfei Zhang [a], Long Chen [a], Haijiao Xie [b], Gang Wang *[a], Tiantian Gu *[a]

[a] *School of Chemistry and Chemical Engineering/State Key Laboratory Incubation Base for Green Processing of Chemical Engineering, Shihezi University, Shihezi 832003, Xinjiang, China*

[b] *Hangzhou Yanqu Information Technology Co., Ltd., Y2, 2nd Floor, Building 2, Xixi Legu Creative Pioneering Park, No. 712 Wen'er West Road, Xihu District, Hangzhou City, Zhejiang Province, 310003, P.R.O.C.*

Corresponding Author

*E-mail: wanggang@shzu.edu.cn (Gang Wang)

*E-mail: hustgutiantian@163.com (Tiantian Gu)

[#]Hong Ding and Tiantian Li contributed equally to this work

Materials synthesis

The material was synthesized from previously reported literature with minor modifications. [1] Synthesis of VN: 225 mg of V_2O_5 (Adamas, 99.5%) powder was added to the mixed solvent of 11 mL NMP (Macklin, 99.5%) and 7 mL deionized water. The above solution was reacted at 140°C for 24 h. The product was filtrated and dried at 80°C for 12 h. The synthesis steps of VNK4, VNK5, VNK10, and VNK20 are consistent with VNK3, except that the m V_2O_5: m KCO (Aladdin, 99%) are 4:1, 5:1, 10:1, and 20:1, respectively. The preparation of V_2O_5-H_2O followed the same procedure as for VN, but the solvent was deionized water without NMP.

Material Characterizations

X-ray diffraction (XRD) characterized the crystal structure of the materials. Fourier transform infrared spectrometer (FTIR) and Raman spectroscope were used to analyze the chemical bonds. The microscopic morphologies were obtained by transmission electron microscope (TEM) and scanning electron microscope (SEM). X-ray photoelectron spectroscopy (XPS) analyzed elemental valence states and species. Thermogravimetry (TG) was used to analyze water and organic matter content.

Electrochemical Measurements

The cathode preparation was to mix 60 wt% product, 30 wt% Ketjen black, and 10 wt% polyvinylidene fluoride. the slurry was loaded onto stainless steel mesh with a loading of about 1–1.5 mg cm^{-2}. The 2032 coin cells were assembled using 2M Zn $(CF_3SO_3)_2$, a GF/C Whatman membrane, and zinc foil. The cyclic voltammetry curves and the discharge/charge test were obtained in 0.2–1.5 V using the CHI604e

electrochemical workstation and the Neware devices (CT-4008T), respectively.

Obtaining layer spacing by Bragg's equation:[2]

$$2d\sin\theta = n\lambda \qquad \text{* MERGEFORMAT (1)}$$

d is the layer spacing, θ is the X-ray incident angle, λ is the X-ray wavelength and n is the positive integer.

Theoretical calculation

The structural optimization of VN, VNK4, and V_2O_5 was carried out by VASP using the Perdew, Burke, and Ernzerhof (PBE) functional and DFT-D3 methods with simultaneous consideration of the spin polarization. The total energy convergence was set as the plane-wave basis with a kinetic energy cutoff of 500 eV, and the Monkhorst-Pack scheme with a k-point grid spacing of 2 π×0.04 $Å^{-1}$ the converged ionic and electronic optimizations conditions were chosen as 0.03 eV/Å and 1×10^{-5} eV, respectively. These complex structures and isolated molecules were optimized using DFT at PBE0-D3/def2-SVP with the implicit solvent model SMD [3] involving water. The structural optimization and vibrational frequency analysis were carried out using B3LYP/TZVP under DFT calculations via Gaussian 16. Meanwhile, the SMD implicit solvent model was used to describe the solvation effect of water. The result analysis, including HOMO-LUMO and ESP, was handled through Multiwfn [4] and VMD [5].

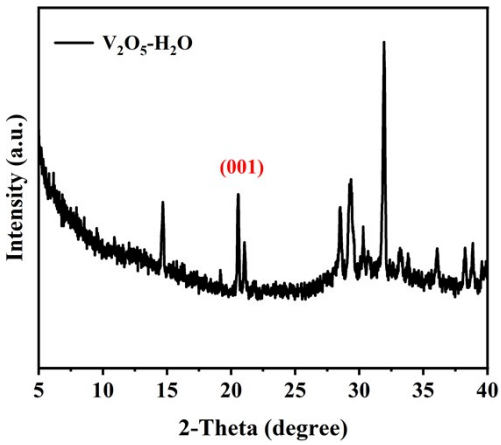

Figure S1. XRD of V_2O_5-H_2O.

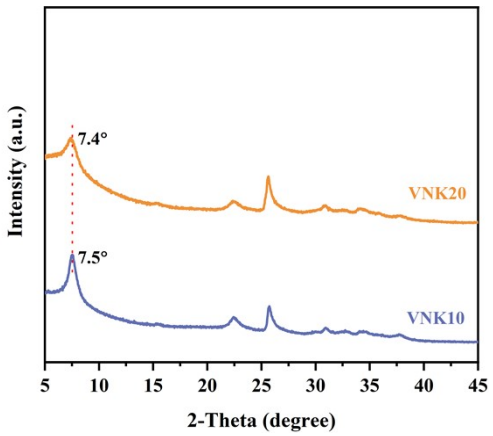

Figure S2. XRD of VNK10 and VNK20.

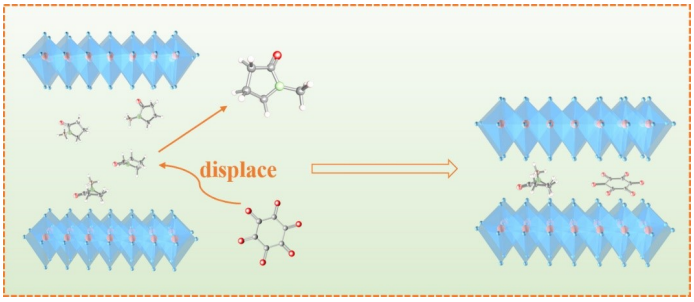

Figure S3. Schematic diagram of KCO replacement of NMP.

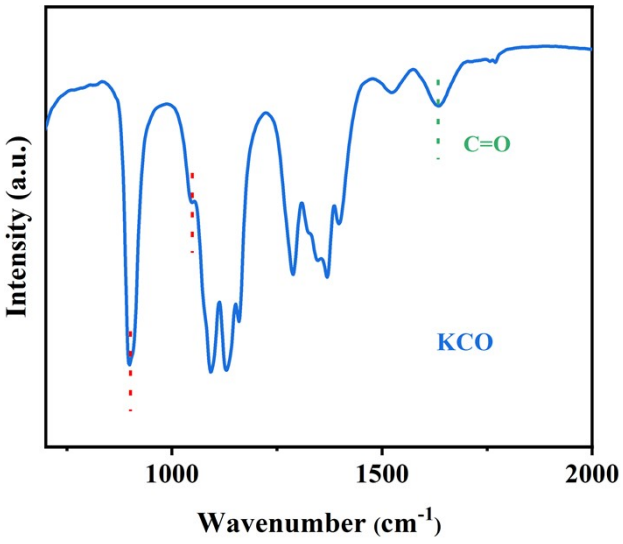

Figure S4. FTIR spectra of KCO.

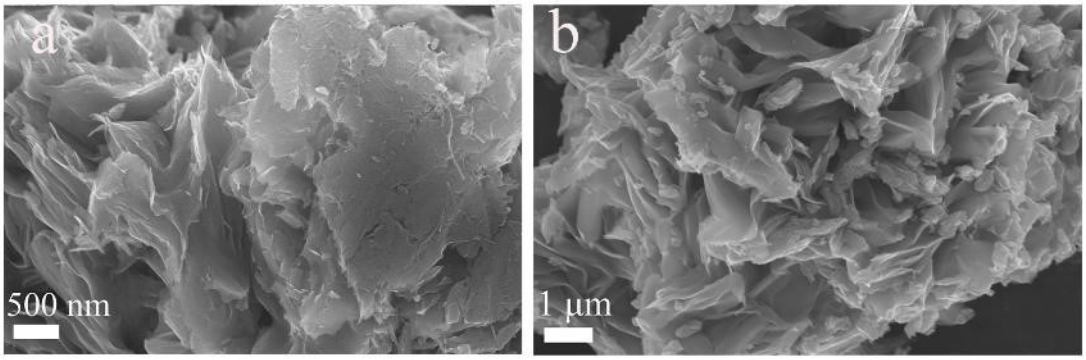

Figure S5. (a-b) SEM images of VNK4.

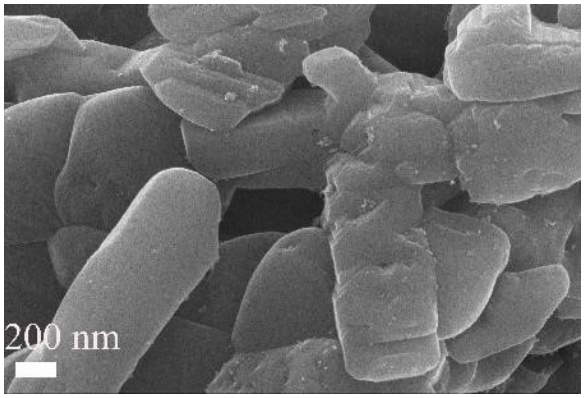

Figure S6. SEM images of commercial V_2O_5.

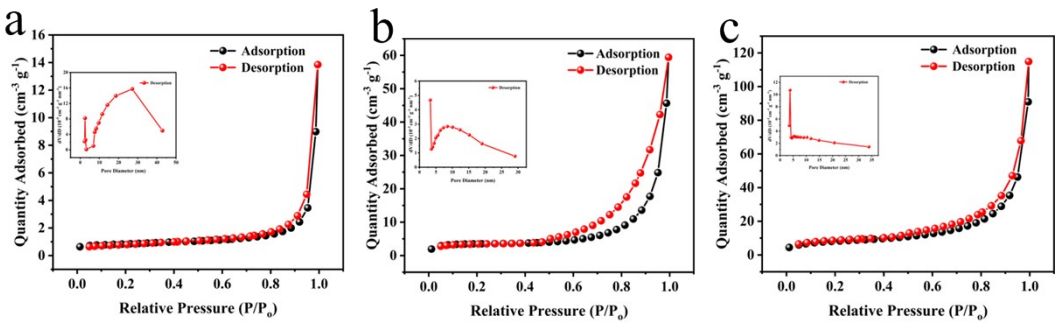

Figure S7. N_2 physisorption isotherms and pore size distribution (inset) of (a) commercial V_2O_5; (b) VN; (c) VNK4

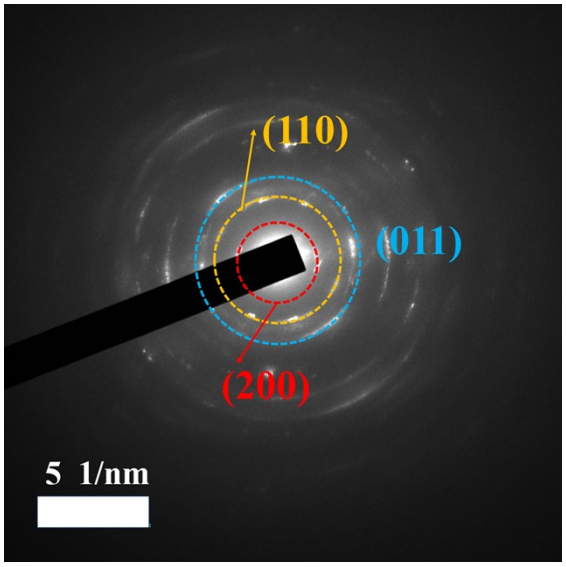

Figure S8. SAED spectrum of VNK4.

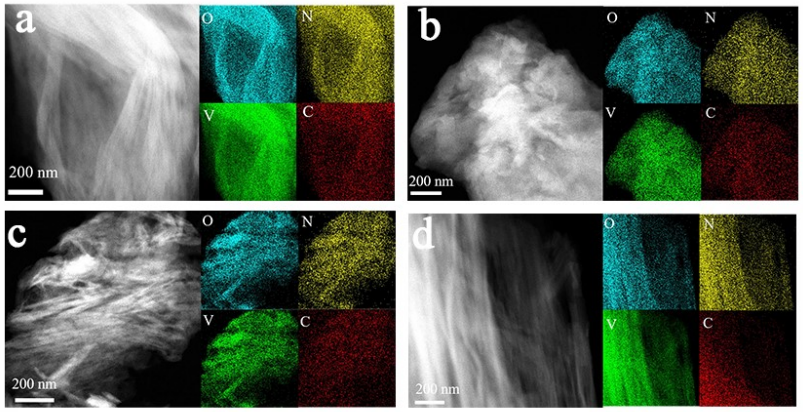

Figure S9. TEM-EDS mapping for (a) VNK4, (b) VN, (c) VNK3, (d) VNK5.

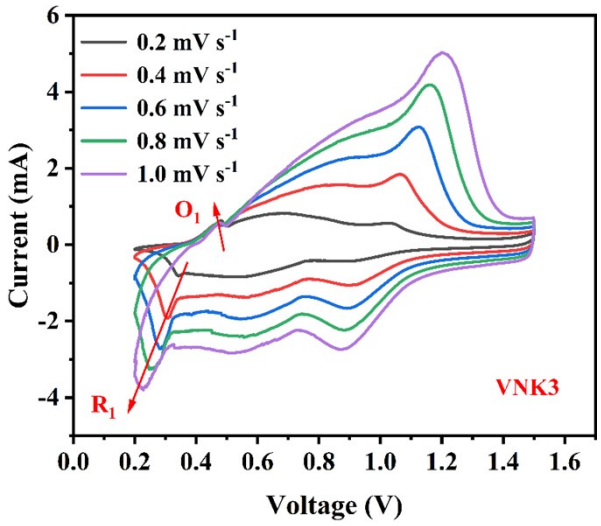

Figure S10. The CV curves of VNK3 at different sweep speeds.

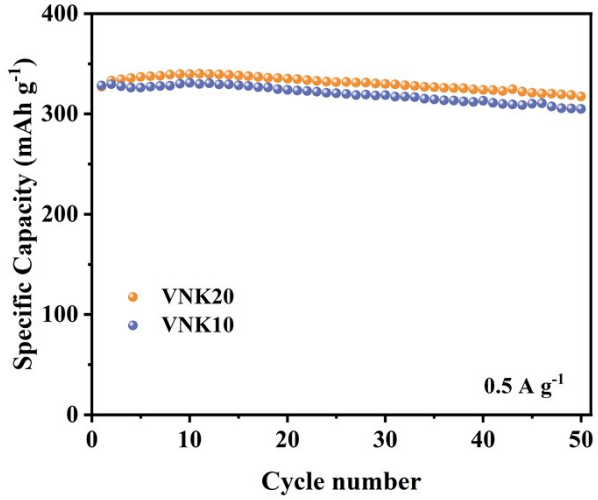

Figure S11. Cycling stability of VNK10 and VNK20 at 0.5 A g^{-1}

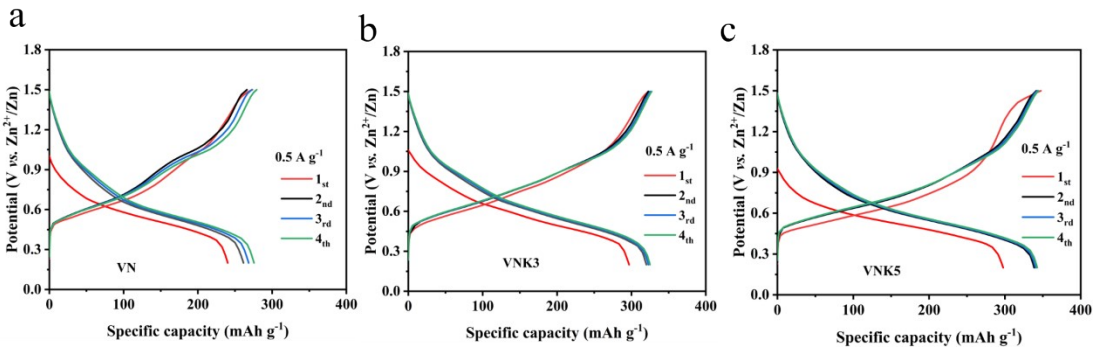

Figure S12. The GCD curves at a current density of 0.5 A g^{-1} of (a) VN, (b) VNK3, (c) VNK5.

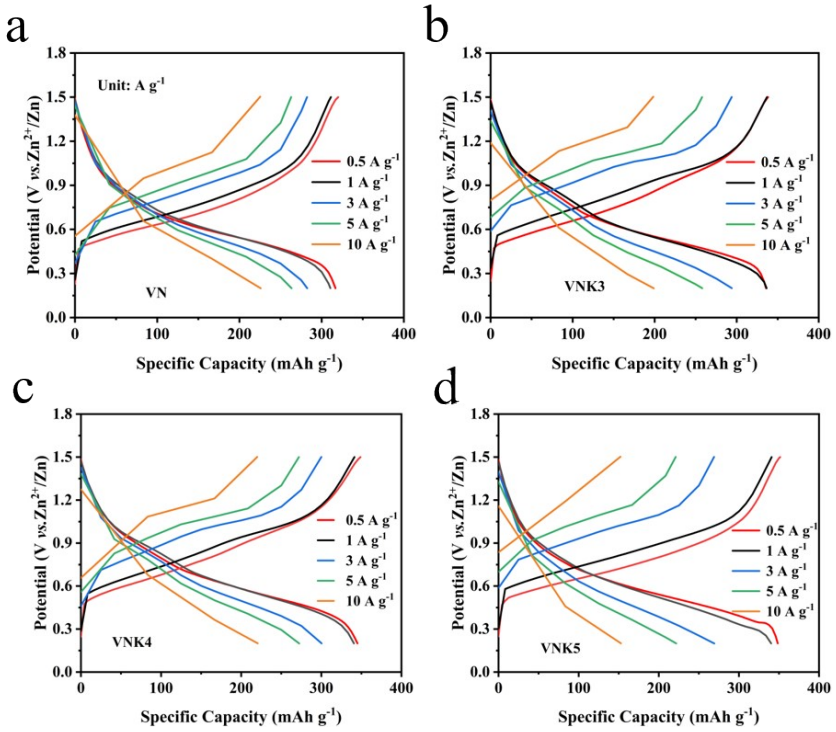

Figure S13. The GCD curves of (a) VN, (b) VNK3, (c) VNK4, (d) VNK5 from 0.5 to 10 A g^{-1}.

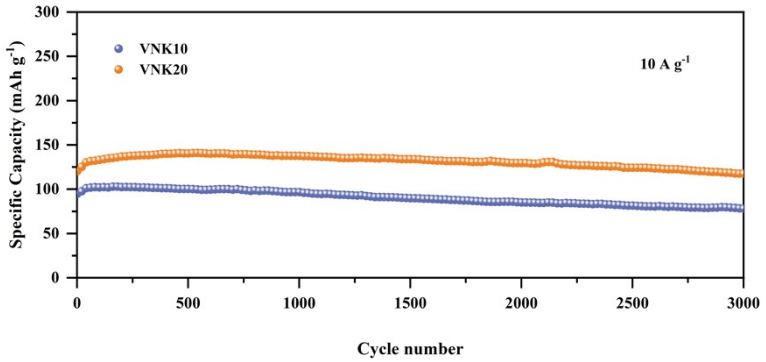

Figure S14. Long-cycle performance of VNK10 and VNK20 at 10 A g^{-1}.

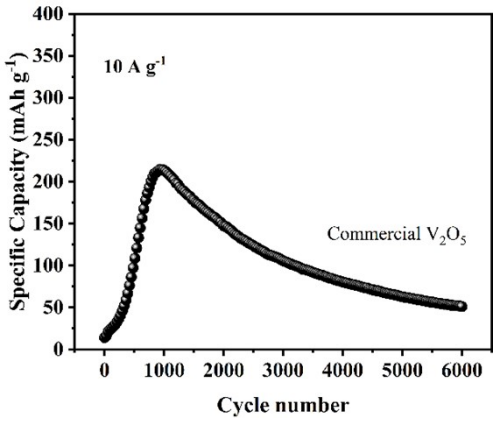

Figure S15. Long-cycle performance of commercial V_2O_5 at 10 A g^{-1}.

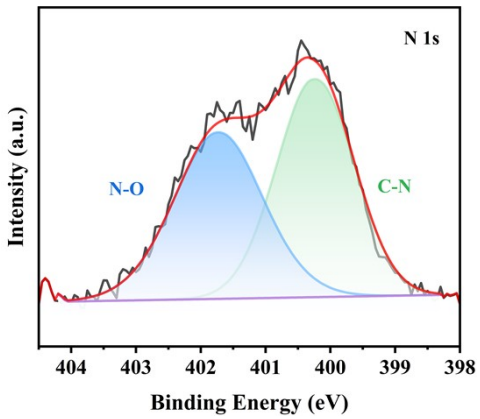

Figure S16. High-resolution spectra of N 1s of VNK4.

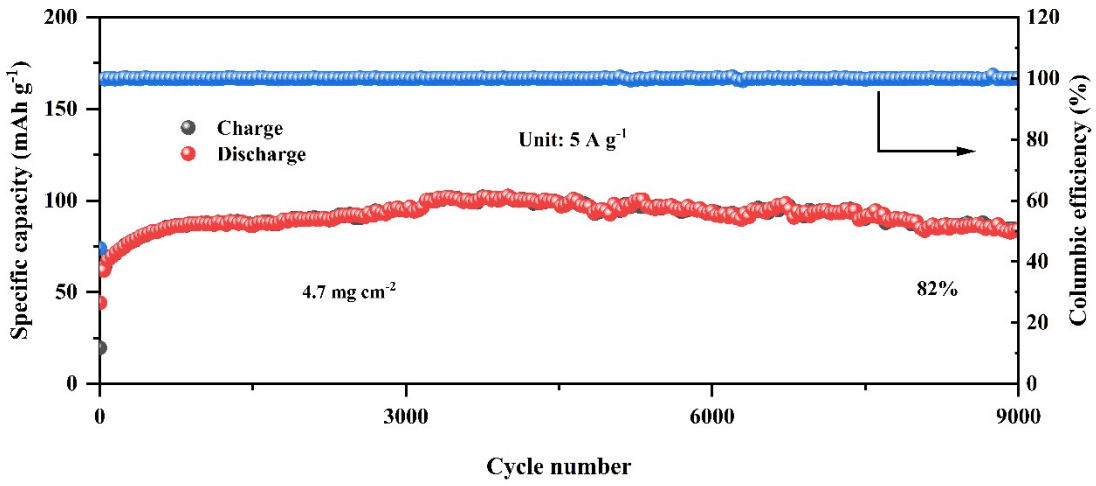

Figure S17. Long-term cycling durability of VNK4 under high load at 5 A g^{-1}.

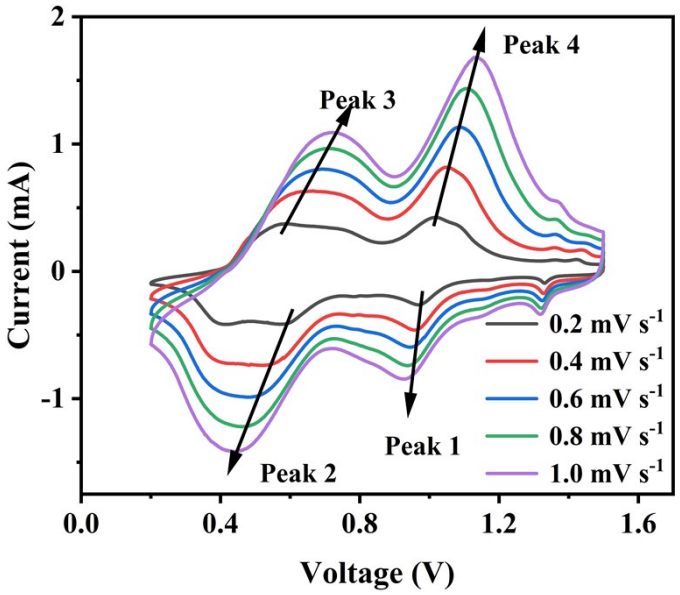

Figure S18. The CV profile of VN at various scan rates.

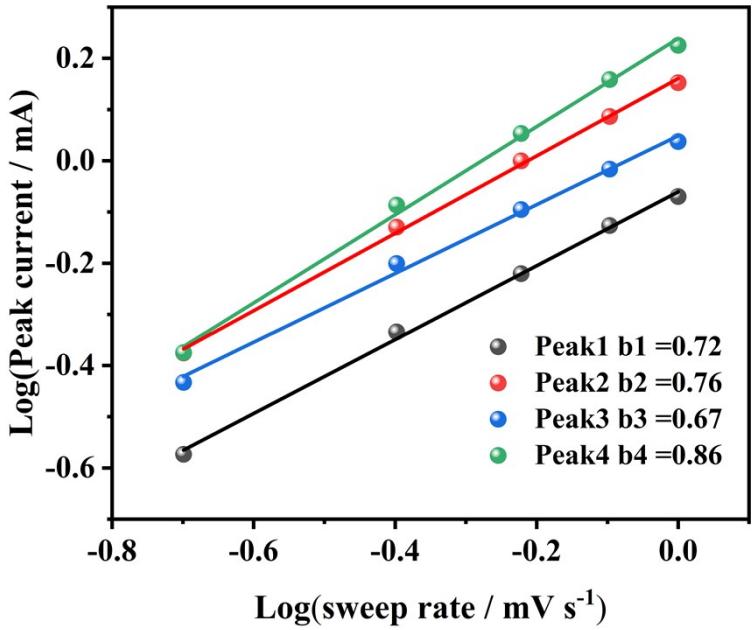

Figure S19. Log (peak current) versus log (scan rate) plots of VN.

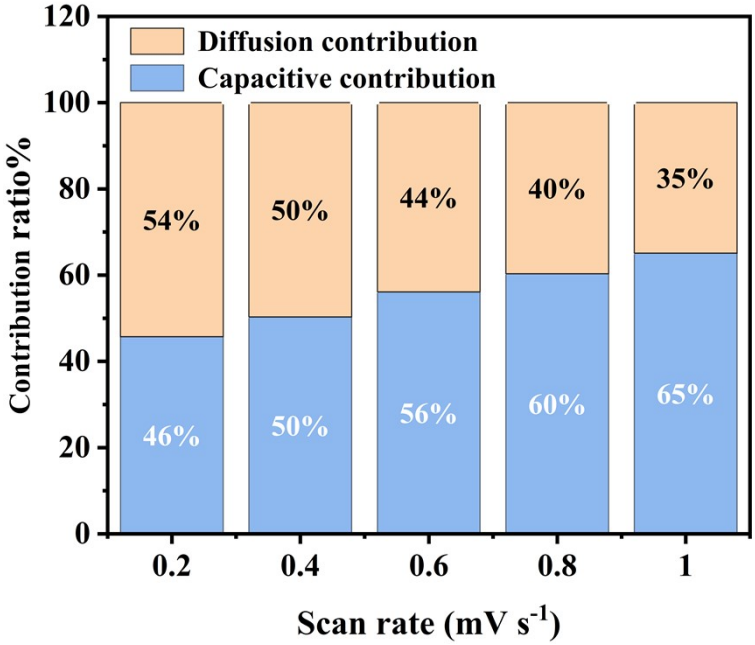

Figure S20. Capacitive contributions of VN at 1.0 mV s^{-1} of VN.

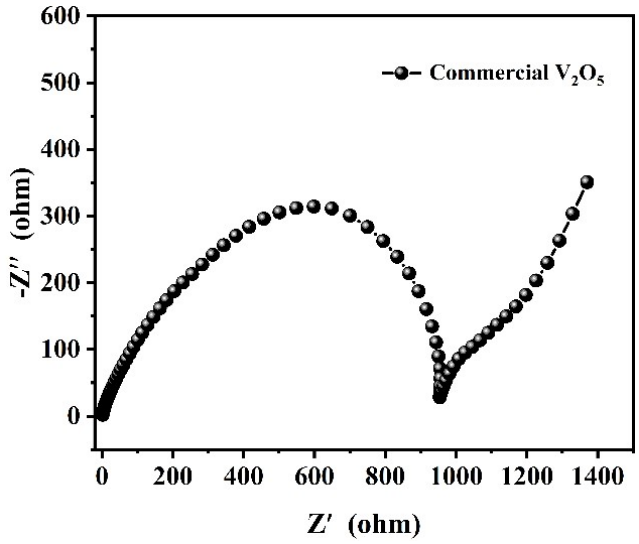

Figure S21. EIS plots of commercial V_2O_5.

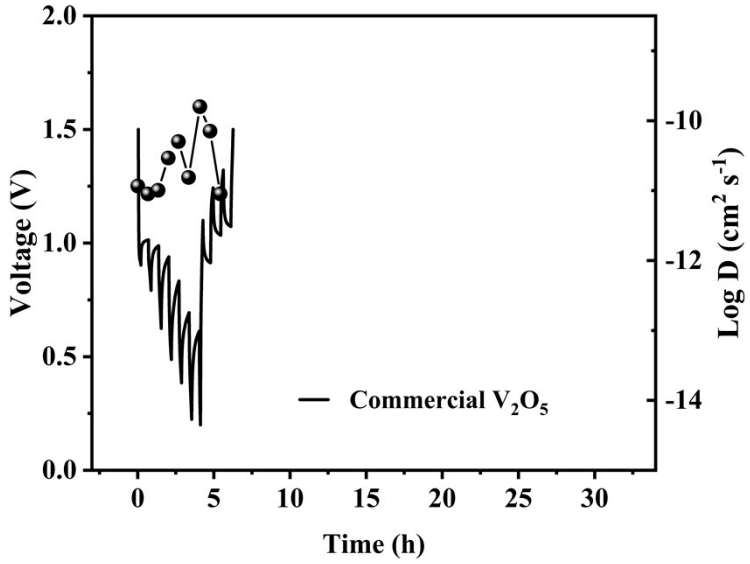

Figure S22. GITT graph of commercial V_2O_5.

For the GITT test, the current pulse of 0.1 A g^{-1} was applied for 10 min, and the relaxation time was 30 min in the voltage window of 0.2-1.5 V.

The diffusion coefficient of Zn^{2+} was obtained according to the below equation. [6, 7]

$$D_{Zn^{2+}} = \frac{4}{\pi\tau}\left(\frac{m_B V_M}{M_B A}\right)^2\left(\frac{\Delta E_S}{\Delta E_\tau}\right)^2 \quad \text{* MERGEFORMAT (2)}$$

Therein, τ denotes the relaxed time of the constant current pulse, m_B, M_B, and V_M mean the weight, moles weight, and mole volume of active materials, respectively. A stands for the area of the electrode-electrolyte contact, ΔE_S denotes the voltage change due to current pulses, and $\Delta E\tau$ represents the voltage change that arises from galvanostatic

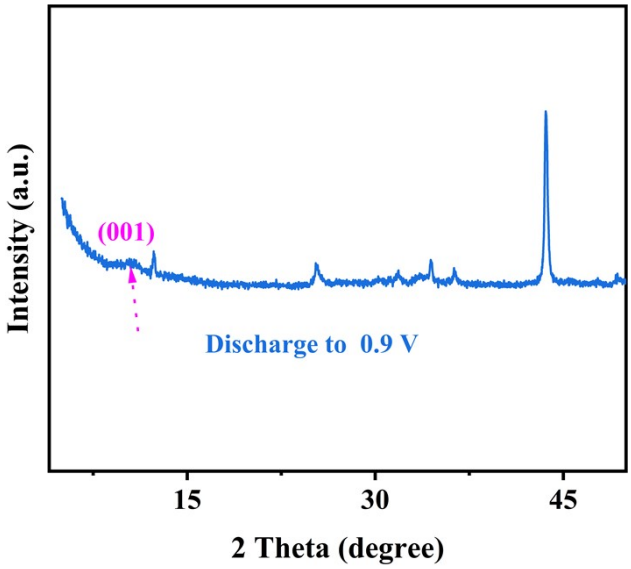

Figure S23. Enlargement of ex-situ XRD spectrum of VNK4 when discharged to 0.9 V.

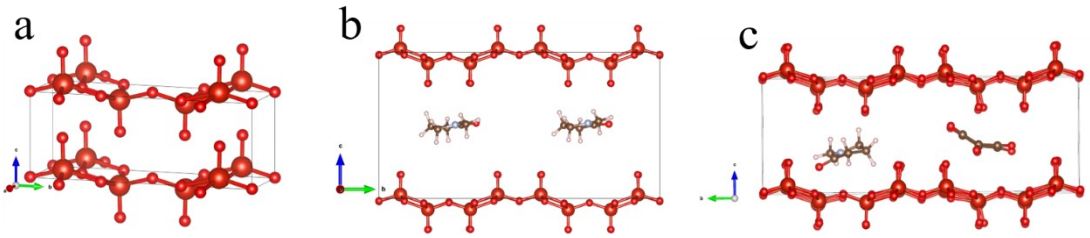

Figure S24. Simulated models for binding energies of (a) commercial V_2O_5, (b) VN, (c) VNK4.

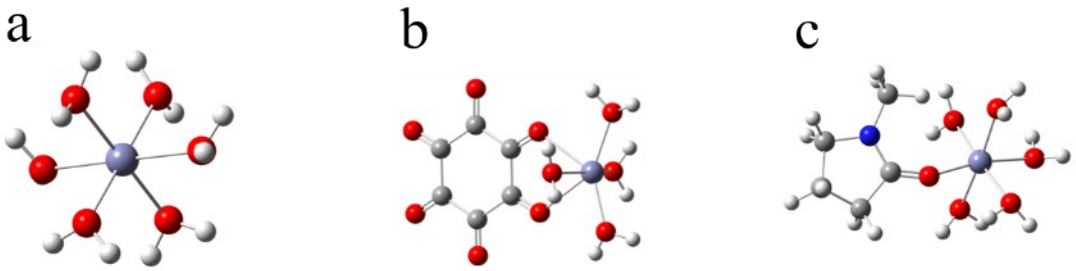

Figure S25. Calculated model for the de-solvation energy of (a)Zn $(H_2O)_6^{2+}$, (b) Zn KCO $(H_2O)_4^{2+}$, (c) Zn NMP $(H_2O)_5^{2+}$.

Table S1. Performance comparison with the organic intercalated vanadium cathodes previously published in the literature.

Materials	Current density	Capacity retention ($mAh\ g^{-1}$)	References
VO-DP	10 A g^{-1}	86.5 (15000 cycles)	[8]
$N(C_4H_9)_4]0.11V_2O_5{\cdot}0.6H_2O$	8 A g^{-1}	142 (3600 cycles)	[9]
(1, 2, 3-BQ)-VO	10 A g^{-1}	204 (3000 cycles)	[10]
HVO-MB	10 A g^{-1}	147 (2000 cycles)	[11]
NiVO-BTA	5 A g^{-1}	241.9 (1600 cycles)	[12]
MO-VOH	3 A g^{-1}	228 (1000 cycles)	[13]
VOH-PPy (PSA)	10 A g^{-1}	165 (5000 cycles)	[14]
NVOY	20 A g^{-1}	170.9 (1500 cycles)	[15]
PANI-VOH	5 A g^{-1}	131 (2000 cycles)	[16]
VNK4	10 A g^{-1}	190.6 (9500 cycles)	**This work**

Reference

1. Y. Xia, X. Wang and J. Zhou, N-Methylpyrrolidone assisted tetrachlorobenzoquinone intercalating V_2O_5 as cathode for aqueous zinc-ion battery, *Chem Commun (Camb)*, 2023, **59**, 6199-6202.
2. K. Zhu, T. Wu, S. Sun, W. van den Bergh, M. Stefik and K. Huang, Synergistic H^+/Zn^{2+} dual ion insertion mechanism in high-capacity and ultra-stable hydrated VO_2 cathode for aqueous Zn-ion batteries, *Energy Storage Mater.*, 2020, **29**, 60-70.
3. A. V. Marenich, C. J. Cramer and D. G. Truhlar, Universal Solvation Model Based on Solute Electron Density and on a Continuum Model of the Solvent Defined by the Bulk Dielectric Constant and Atomic Surface Tensions, *The Journal of Physical Chemistry B*, 2009, **113**, 6378-6396.
4. T. Lu and F. Chen, Multiwfn: a multifunctional wavefunction analyzer, *J Comput Chem*, 2012, **33**, 580-592.
5. W. Humphrey, A. Dalke and K. Schulten, VMD: Visual molecular dynamics, *Journal of Molecular Graphics*, 1996, **14**, 33-38.
6. Q. Zong, Y. Zhuang, C. Liu, Q. Kang, Y. Wu, J. Zhang, J. Wang, D. Tao, Q. Zhang and G. Cao, Dual Effects of Metal and Organic Ions Co-Intercalation Boosting the Kinetics and Stability of Hydrated Vanadate Cathodes for Aqueous Zinc-Ion Batteries, *Adv. Energy Mater.*, 2023, **13**, 2301480.
7. Y. Liu, T. Wang, Y. Sun, M. Zhang, G. Gao, J. Yang and K. Cai, Fast and efficient in-situ construction of low crystalline PEDOT-intercalated V_2O_5

nanosheets for high-performance zinc-ion battery, *Chem. Eng. J*, 2024, **484**, 149501.

8. M. Zhang, X. Zhang, Q. Dong, S. Zhang, Z. Xu, Z. Hou and Y. Qian, Organic Molecular Intercalated $V_3O_7{\cdot}H_2O$ with High Operating Voltage for Long Cycle Life Aqueous Zn-Ion Batteries, *Adv. Funct. Mater.*, 2023, **33**, 2213187.
9. M. Zhu, H. Wang, W. Lin, D. Chan, H. Li, K. Wang, Y. Tang, T. Hao, S. Chen, O. I. Malyi, Y. Tang and Y. Zhang, Amphipathic Molecules Endowing Highly Structure Robust and Fast Kinetic Vanadium-Based Cathode for High-Performance Zinc-Ion Batteries, *Small Structures*, 2022, **3**, 2200016.
10. K. Li, Y. Gong and J. Lin, Benzoquinone-intercalated vanadium oxide in the electrolyte with Al^{3+} for zinc-ion storage: dual-pillar effect and reversible disorder–order conversion, *Chem. Eng. J*, 2023, **452**, 139621.
11. Y. Tong, Y. Zang, S. Su, Y. Zhang, J. Fang, Y. Yang, X. Li, X. Wu, F. Chen, J. Hou and M. Luo, Methylene blue intercalated vanadium oxide with synergistic energy storage mechanism for highly efficient aqueous zinc ion batteries, *J. Energy Chem.*, 2023, **77**, 269-279.
12. J. Guo, J. Liu, W. Ma, Z. Sang, L. Yin, X. Zhang, H. Chen, J. Liang and D. a. Yang, Vanadium Oxide Intercalated with Conductive Metal-Organic Frameworks with Dual Energy-Storage Mechanism for High Capacity and High-Rate Capability Zn Ion Storage, *Adv. Funct. Mater.*, 2023, **33**, 2302659.
13. R. Cui, J. Gu, N. Wang, Y. Wang, X. Huang, S. Zhang, L. Lu and D. Wang, Organic Dye Molecule Intercalated Vanadium Oxygen Hydrate Enables High-

Performance Aqueous Zinc-Ion Storage, *Small*, 2024, **20**, 2307849.

14. Z. Feng, J. Sun, Y. Liu, H. Jiang, M. Cui, T. Hu, C. Meng and Y. Zhang, Engineering Interlayer Space of Vanadium Oxide by Pyridinesulfonic Acid-Assisted Intercalation of Polypyrrole Enables Enhanced Aqueous Zinc-Ion Storage, *ACS Appl. Mater. Interfaces*, 2021, **13**, 61154-61165.

15. Y. Gong, P. Zhang, S. Fan, M. Cai, J. Hu, Z. Luo, H. Mi, X. Jiang, Q. Zhang and X. Ren, Polypyrrole pre-intercalation engineering-induced NH_4^+ removal in tunnel ammonium vanadate toward high-performance zinc ion batteries, *J. Colloid Interface Sci.*, 2024, **664**, 168-177.

16. Y. Zhang, L. Xu, H. Jiang, Y. Liu and C. Meng, Polyaniline-expanded the interlayer spacing of hydrated vanadium pentoxide by the interface-intercalation for aqueous rechargeable Zn-ion batteries, *J. Colloid Interface Sci.*, 2021, **603**, 641-650.